Inorganic Chemistry

Article

pubs.acs.org/IC

A Convenient Route to Synthetic Analogues of the Oxidized Form of High-Potential Iron–Sulfur Proteins

Kazuki Tanifuji,[†] Norihiro Yamada,[†] Tomoyuki Tajima,[†] Takahiro Sasamori,[‡] Norihiro Tokitoh,[‡] Tsukasa Matsuo,[§,∥] Kohei Tamao,[§] Yasuhiro Ohki,[†] and Kazuyuki Tatsumi*[,†]

[†]Department of Chemistry, Graduate School of Science, and Research Center for Materials Science, Nagoya University, Furo-cho, Chikusa-ku, Nagoya 464-8602, Japan

[‡]Institute for Chemical Research, Kyoto University, Gokasho, Uji, Kyoto 611-0011, Japan

[§]Functional Elemento-Organic Chemistry Unit, RIKEN Advanced Science Institute, 2-1 Hirosawa, Wako, Saitama 351-0198, Japan

[∥]Department of Applied Chemistry, Faculty of Science and Engineering, Kinki University, 3-4-1 Kowakae, Higashi-Osaka, Osaka 577-8502, Japan

Supporting Information

ABSTRACT: An amide-bound $[Fe_4S_4]^{3+}$ cluster, $[Fe_4S_4\{N(SiMe_3)_2\}_4]^-$ (**1**), was found to serve as a convenient precursor for synthetic analogues of the oxidized form of high-potential iron–sulfur proteins. Treatment of **1** with 4 equiv of bulky thiols led to replacement of the amide ligands with thiolates, giving rise to a series of $[Fe_4S_4(SR)_4]^-$ clusters (R = Dmp (**2a**), Tbt (**2b**), Eind (**2c**), Dxp (**2d**), Dpp (**2e**); Dmp = 2,6-di(mesityl)phenyl, Tbt = 2,4,6-tris[bis(trimethylsilyl)methyl]phenyl, Eind = 1,1,3,3,5,5,7,7-octaethyl-*s*-hydrindacen-4-yl, Dxp = 2,6-di(*m*-xylyl)phenyl, Dpp = 2,6-diphenylphenyl). These clusters were characterized by the mass spectrum, the EPR spectrum, and X-ray crystallography. The redox potentials of the $[Fe_4S_4]^{3+/2+}$ couple, −0.82 V (**2a**), −0.86 V (**2b**), −0.84 V (**2c**), −0.74 V (**2d**), and −0.63 V (**2e**) vs Ag/Ag^+ in THF, are significantly more negative than that of $[Fe_4S_4(SPh)_4]^{-/2-}$ (−0.21 V).

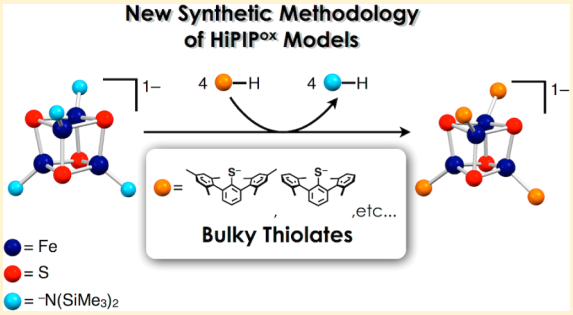

INTRODUCTION

The $[Fe_4S_4]$ clusters are abundant cofactors of metalloproteins in biological electron-transfer sequences, and these clusters exhibit multiple oxidation states with a small structural change.[1] Two major families are known for electron-transfer proteins with an $[Fe_4S_4]$ cluster: the ferredoxin (Fd) family and the high-potential iron–suflur protein (HiPIP) family. Their $[Fe_4S_4]$ cores are ligated by four cysteinyl thiolates (Cys) from the protein backbone, forming $[Fe_4S_4(Cys)_4]$. Although the $[Fe_4S_4(Cys)_4]$ cluster is common to Fd and HiPIP, the redox couples used in these proteins are different, $[Fe_4S_4]^{2+}/[Fe_4S_4]^+$ for Fd and $[Fe_4S_4]^{3+}/[Fe_4S_4]^{2+}$ for HiPIP. The difference in the operating redox couples has been attributed to the environment around the $[Fe_4S_4]$ cluster. The smaller number of hydrogen bonds between water and the $[Fe_4S_4]$ cluster of HiPIP has been proposed to account for the stability of the $[Fe_4S_4]^{3+}$ state,[2] and the crystal structures of HiPIP have revealed hydrophobic binding pockets for the $[Fe_4S_4]$ cluster.[3] However, a wide range of $[Fe_4S_4]^{3+}/[Fe_4S_4]^{2+}$ redox potentials has been observed for HiPIPs, from +50 mV to +500 mV vs NHE,[4] and the factors contributing to the variety of redox potentials remain in discussion.[3f]

Synthetic analogues of $[Fe_4S_4]$ clusters have provided insights into the structures and the properties of the clusters in proteins. Thus far, more than 70 examples of $[Fe_4S_4]^{2+}$ clusters, $[Fe_4S_4(SR)_4]^{2-}$ (SR = thiolates), and around 10 examples of $[Fe_4S_4]^+$ clusters, $[Fe_4S_4(SR)_4]^{3-}$, have been reported,[5] and comparisons of their properties have been useful to evaluate the correlation of hydrogen bonding,[6] the net charge of the clusters,[7] solvents,[8] and bulkiness of ligands[9] to the redox potentials and the accessible oxidation states of these clusters. On the other hand, $[Fe_4S_4(STip)_4]^-$ (Tip = 2,4,6-triisopropylphenyl) has been the only isolated $[Fe_4S_4]^{3+}$ cluster modeling the oxidized form of HiPIP until recently.[10] We[11] and Lee et al.[12] have recently synthesized the amide-ligated $[Fe_4S_4]^{3+}$ cluster $[Fe_4S_4\{N(SiMe_3)_2\}_4]^-$ (**1**) from one-electron reduction of the all-ferric cluster $Fe_4S_4\{N(SiMe_3)_2\}_4$.[13] The $N(SiMe_3)_2$ group is known to serve as a Br*ϕ*nsted base, and we have demonstrated that treatment of an $Fe–N(SiMe_3)_2$ moiety with various thiols results in ligand exchange from an amide to a thiolate.[14] Similar ligand exchange was observed in the reaction of **1** with 4 equiv of HSDmp (Dmp = 2,6-di(mesityl)phenyl), where the second isolated model of the oxidized form of HiPIP, $[Fe_4S_4(SDmp)_4]^-$ (**2a**), was obtained.[11] The successful synthesis of **2a** from the reaction

Received: November 21, 2013
Published: April 2, 2014

of **1** with HSDmp prompted us to expand the scope of this reaction to synthesize various clusters modeling the oxidized form of HiPIP. In this paper, we report the synthesis and properties of a series of $[Fe_4S_4]^{3+}$ clusters, $[Fe_4S_4(SR)_4]^-$ (R = Tbt (**2b**), R = Eind (**2c**), R = Dxp (**2d**), R = Dpp (**2e**); Tbt = 2,4,6-tris[bis(trimethylsilyl)methyl]phenyl, Eind = 1,1,3,3,5,5,7,7-octaethyl-*s*-hydrindacen-4-yl, Dxp = 2,6-di(*m*-xylyl)phenyl, Dpp = 2,6-di(phenyl)phenyl).

RESULTS AND DISCUSSION

Synthesis of $[Fe_4S_4]^{3+}$ Clusters. Treatment of $[Na(THF)_2][Fe_4S_4\{N(SiMe_3)_2\}_4]$ ($[Na(THF)_2]$**1**) with 4 equiv of bulky thiols (HSR) in toluene led to the formation of the $[Fe_4S_4]^{3+}$ clusters, $[Fe_4S_4(SR)_4]^-$ (**2a**–**e**) (Scheme 1).

Scheme 1

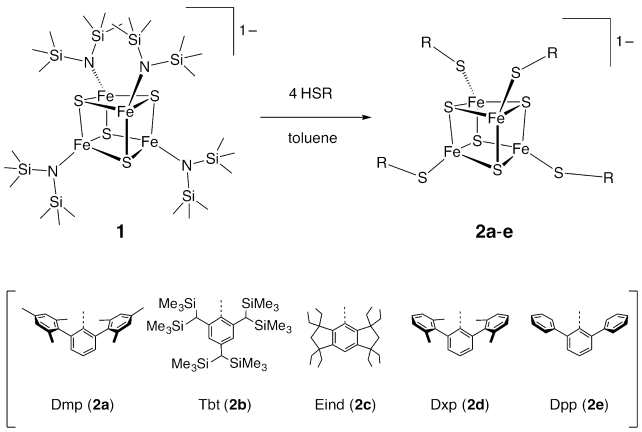

Subsequent cation exchange from $[Na]^+$ to $[N^nBu_4]^+$ was carried out for **2a** and **2c**–**e** by treatment with $[N^nBu_4][PF_6]$ in THF. The crystal yields of **2a**–**e**, either with Na or with N^nBu_4 cations, range from 26% to 72% depending on their readiness to crystallize, while the dominant formation of $[Fe_4S_4(SR)_4]^-$ was observed in the electrospray ionization mass spectrum (ESI-MS) of the reaction mixtures where the anionic signals appeared at m/z = 1732.4 (**2a**), 2006.1 (**2c**), 1620.4 (**2d**), and 1396.4 (**2e**), as shown in Figure 1 for the mixture of **1** and 4 equiv of HSDmp. An exception was the reaction mixture of **1** and HSTbt, from which no significant ESI-MS signal for the iron–sulfur cluster was detected in the range of m/z = 500–3000. The absence of the signal of **2b** in the ESI-MS may be due to efficient capture of the Na cation by the STbt group and the $[Fe_4S_4]$ core, hindering the separation of the Na cation from the cluster anion. The reaction depicted in Scheme 1 demonstrates a convenient and clean synthetic route to less common $[Fe_4S_4]^{3+}$ clusters, which are now readily accessible by changing the thiols to be added to **1**.

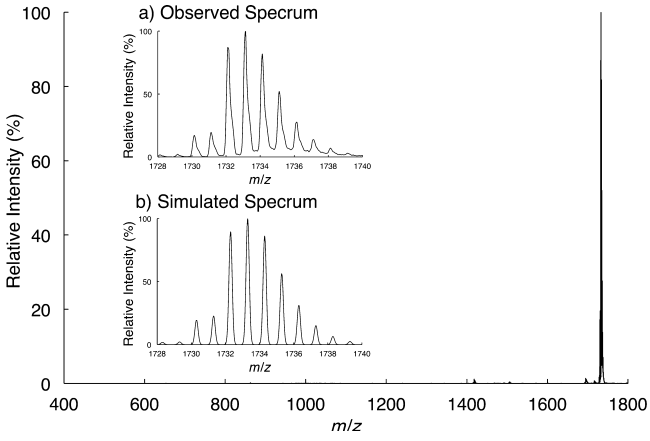

Figure 1. ESI-MS spectrum of the reaction mixture of **1** + 4HSDmp. The insets show (a) the observed and (b) the simulated spectrum of the range between m/z = 1728 and 1740. The reaction mixture in toluene was diluted with THF for measurement.

Less polar organic solvents, such as toluene and THF, appeared to be crucial for this reaction. Although the reactions performed in CH_3CN gave $[Fe_4S_4(SR)_4]^-$ as the initial product, the ESI-MS of the CH_3CN solution gradually exhibited the signals of thiolates (^-SR), $[Fe_4S_4(SR)_4]^{2-}$, and other unidentified anions as time passed. Dimethylformamide (DMF) and methanol, which are often used as solvents in the synthesis of $[Fe_4S_4]$ clusters, reacted rapidly with **1** to give unidentified products. Furthermore, clusters **2a**–**e** appeared to be unstable when dissolved in DMF or methanol. A similar observation was reported by Millar et al., who found that the stability of $[Fe_4S_4(STip)_4]^-$ is in the following order, CH_2Cl_2 > $CH_3CN \gg$ DMF.[10] This trend is consistent with the ascending order of the donor number (Lewis basicity) of these solvents, and hence degradation of $[Fe_4S_4(SR)_4]^-$ may be triggered by the coordination of polar organic solvents to iron.

The use of bulky thiols appeared to be important for the successful synthesis of $[Fe_4S_4(SR)_4]^-$ (**2a**–**e**), partly because the bulky thiolate ligands would hinder the access of solvents to the iron center. Another advantage of introducing bulky thiolates is the high solubility of $[Fe_4S_4(SR)_4]^-$ into less polar organic solvents. Bulky alkyl-thiolates $-S^tBu$ and $-SC(SiMe_3)_3$ are applicable for the synthesis of $[Fe_4S_4(SR)_4]^-$ (R = ^{t}Bu, $C(SiMe_3)_3$) from **1** and HSR in THF. The ESI-MS signals of $[Fe_4S_4(SR)_4]^-$ appeared at m/z = 707.8 (R = ^{t}Bu) and 1406.1 (R = $C(SiMe_3)_3$), while crystallization of these clusters has been unsuccessful. On the other hand, the reaction mixtures of **1** and less bulky thiols, such as HSPh, $HS(C_6H_4$-4-^{t}Bu), HS^{i}Pr, and HSEt, did not show the ESI-MS signals of $[Fe_4S_4(SR)_4]^-$, and the subsequent work-up gave unidentified products.

Absorption Spectra and EPR Spectra of $[Fe_4S_4]^{3+}$ Clusters. The absorption spectra of clusters **2a**, **2c**, and **2d** exhibited two bands in the ranges of 342–348 nm and 446–502 nm, while a single absorption maximum was observed for **2b** and **2e** at 459–465 nm (Table 1). These absorptions are assignable to the ligand-to-metal charge transfer (LMCT) bands.[15] The absorption maxima of **2a**, **2c**, and **2d** (λ_{max} = 342–348 nm, 446–502 nm) are slightly lower in energy compared with those for the $[Fe_4S_4]^{3+}$ cluster $[Fe_4S_4(SAd)_4]^-$ (λ_{max} = 326, 430 nm, Ad = adamantyl), which was generated in situ via electrochemical oxidation of $[Fe_4S_4(SAd)_4]^{2-}$ (λ_{max} = 318, 418 nm).[9] Comparison of the absorptions for $[Fe_4S_4(SAd)_4]^{-/2-}$ indicates the red-shift of absorption maxima upon oxidation, and this is also the case for $[Fe_4S_4\{N(SiMe_3)_2\}_4]^{n-}$ (n = 0, 1, 2)[12] and the $[Fe_4S_4]$ cluster of *Rhodothermus marinus* HiPIP.[3f]

Clusters **2a**–**e** indicated the S = 1/2 ground state in the EPR spectrum, as shown in Figure 2 for $[Na(THF)]$**2a** (g = 2.076, 2.035, 2.018). As summarized in Table 1, the EPR signals of other clusters appeared as rhombic for $[N^nBu_4]$**2a** (g = 2.100, 2.051, 2.021) and $[N^nBu_4]$**2c** (g = 2.136, 2.043, 2.025) and axial for $[Na(THF)]$**2b** (g = 2.100, 2.041), $[N^nBu_4]$**2d** (g = 2.109, 2.051), and $[N^nBu_4]$**2e** (g = 2.071, 2.028). The averaged g values, g_{avg} = 2.043 ($[Na(THF)]$**2a**), 2.057 ($[N^nBu_4]$**2a**), 2.061

dx.doi.org/10.1021/ic402890k | *Inorg. Chem.* 2014, 53, 4000–4009

Table 1. Absorption Maxima and EPR Data of $[Fe_4S_4]^{3+}$ Clusters 2a−e

	λ_{max}, nm (ε, M^{-1} cm^{-1})[a]		g values	g_{avg}
[Na(THF)]**2a**	348 (1.7×10^4)	446 (1.4×10^4)	2.076, 2.035, 2.018[b]	2.043
[N^nBu_4]**2a**	343 (2.1×10^4)	469 (2.3×10^4)	2.100, 2.051, 2.021[b]	2.057
[Na(THF)]**2b**		459 (2.0×10^4)	2.100, 2.041[b]	2.061
[N^nBu_4]**2c**	342 (1.4×10^4)	502 (3.1×10^4)	2.136, 2.043, 2.025[c]	2.068
[N^nBu_4]**2d**	344 (2.2×10^4)	466 (2.6×10^4)	2.109, 2.051[c]	2.070
[N^nBu_4]**2e**		465 (2.1×10^4)	2.071, 2.028[c]	2.042

[a]Measured in THF. [b]Measured at 8 K. [c]Measured at 16 K.

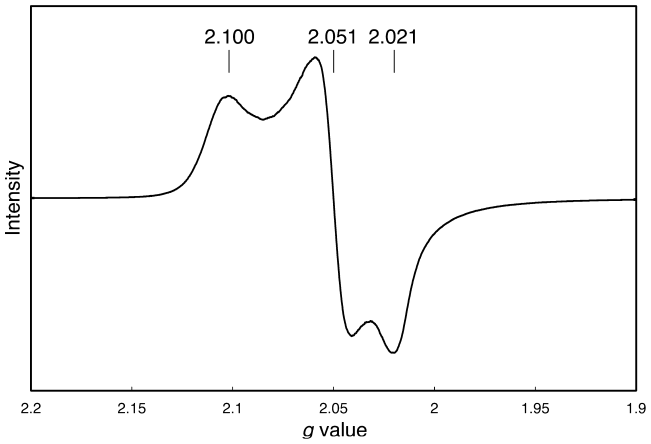

Figure 2. EPR spectrum (X band, microwave 1.0 mW) of [N^nBu_4]**2a** measured in frozen toluene at 8 K.

([Na(THF)]**2b**), 2.068 ([N^nBu_4]**2c**), 2.070 ([N^nBu_4]**2d**), and 2.042 ([N^nBu_4]**2e**), are comparable to that of $[Fe_4S_4(STip)_4]^-$ (g_{avg} = 2.06, g = 2.10, 2.05, 2.03)[16] and are higher than those of $[Fe_4S_4(SR)_4]^{3-}$, g_{avg} = 1.97 (R = CH_2Ph) and 1.97 (R = Ph).[17] These results are consistent with the EPR observation on *Rhodophia globiformis* HiPIP, where the g_{avg} value is higher for the $[Fe_4S_4]^{3+}$ state (g_{avg} = 2.08, g = 2.12, 2.03) than for the $[Fe_4S_4]^+$ state (g_{avg} = 1.98, g = 2.04, 1.92).[18] The g_{avg} values for the $[Fe_4S_4]^{3+}$ state of other HiPIPs are 2.056 (*Rhodopseudomonas gelatinosa*),[19] 2.065 (*Thiobacillus ferrooxidans*),[20] and 2.069 (*Ectothiorhodospiza halophila*),[21] which are also comparable to those of clusters **2a**−**e**.

Structures of $[Fe_4S_4]^{3+}$ Clusters. Single crystals of clusters **2a**−**e** suitable for X-ray crystallography were obtained with Na (**2a**, **2b**) or N^nBu_4 (**2a**, **2c**, **2d**, **2e**) countercations. The structures of [Na(THF)]**2a**, [Na(THF)]**2b**, and [N^nBu_4]**2c** are shown in Figure 3.

The Na(THF) groups of [Na(THF)]**2a** (R = Dmp) and [Na(THF)]**2b** (R = Tbt) are disordered over two and four positions, respectively, and only one of each type of group is shown for clarity. The coordination geometry of Na varies depending on the thiolate substituent, because the *m*-terphenyl groups (R = Dmp, Dxp, Dpp) offer a possible interaction between Na and one of the aryl moieties attached to the 2,6-positions of the central ring. For example, the Na cation of [Na(THF)]**2a** is in a distorted tetrahedral geometry, interacting with an oxygen atom of THF, two sulfur atoms of SDmp, and the $[Fe_4S_4]$ core, in addition to one of the mesityl rings of the Dmp group. On the other hand, the Na cation in [Na(THF)]**2b** is in a distorted T-shape geometry, with the S(core)−Na−O, S(core)−Na−S(thiolate), and S(thiolate)−Na−O angles being 156.2(4)°, 77.0(3)°, and 126.3(5)°, respectively. An additional C−H···Na interaction may be present, if the shortest C···Na distance of 2.7661(4) Å is taken into account. In the cases of [N^nBu_4]**2a**, [N^nBu_4]**2c** (R = Eind), [N^nBu_4]**2d** (R = Dxp), and [N^nBu_4]**2e** (R = Dpp), weak C−H···S hydrogen bonds may be present between the N^nBu_4 cation and sulfur atoms of thiolates or the $[Fe_4S_4]$ core, with the shortest C···S distances of 3.512(2)−3.733(4) Å, while some of these distances are longer than the structurally identified C−H···S hydrogen bond (C···S, 3.649(3) Å) found for 2,3-diphenyl-4-morpholinomethyl-5-ehynyl-2-thio-2-phosphabicyclo[4.4.0]decan-5-ol.[22]

The iron atoms of clusters **2a**−**e** are in a distorted tetrahedral geometry, coordinated by three sulfur atoms of the $[Fe_4S_4]$ core and one thiolate sulfur. The mean Fe−Fe and Fe−S(core)

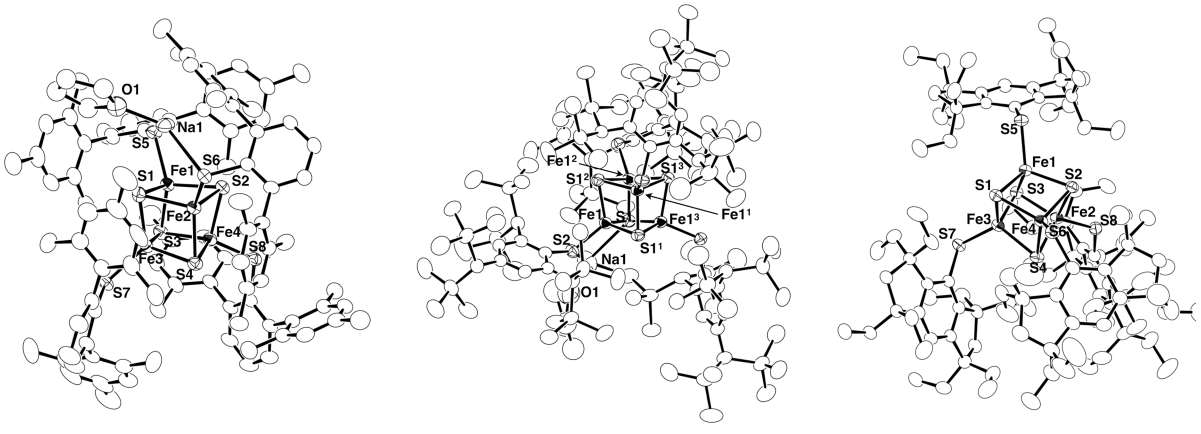

Figure 3. Structures of [Na(THF)]**2a** (left), [Na(THF)]**2b** (center), and [N^nBu_4]**2c** (right) with thermal ellipsoids at the 50% probability level. The Na(THF) group of [Na(THF)]**2a** and [Na(THF)]**2b** is disordered (see text), and one of each is shown for clarity. The [N^nBu_4] cation of [N^nBu_4]**2c** is omitted for clarity.

dx.doi.org/10.1021/ic402890k | *Inorg. Chem.* 2014, 53, 4000−4009

Table 2. Averaged Bond Distances (Å) for Clusters 2a–e, $[Fe_4S_4(STip)_4]^-$, $[Fe_4S_4(SDpp)_4]^{2-}$, $[Fe_4S_4(SMes)_4]^{2-}$, $[Fe_4S_4(SPh)_4]^{2-}$, and $[Fe_4S_4(SPh)_4]^{3-}$

	[Na(THF)]**2a**	[N^{n}Bu$_4$]**2a**	**2b**	**2c**
oxidation state		$[Fe_4S_4]^{3+}$		
avg Fe–Fe	2.7677(10)	2.7846(9)	2.7854(7)	2.7685(8)
avg Fe–S(core)	2.2688(14)	2.2691(15)	2.2819(11)	2.2661(11)
avg Fe–S(thiolate)	2.2268(11)	2.2439(13)	2.2423(11)	2.2308(11)
avg S(thiolate)–C	1.784(6)	1.785(5)	1.786(3)	1.792(4)
	2d	**2e**	$[Fe_4S_4(STip)_4]^{-a}$	$[Fe_4S_4(SDpp)_4]^{2-b}$
oxidation state	$[Fe_4S_4]^{3+}$	$[Fe_4S_4]^{3+}$	$[Fe_4S_4]^{3+}$	$[Fe_4S_4]^{2+}$
avg Fe–Fe	2.7985(10)	2.7324(4)	2.74(1)	2.759(2)
avg Fe–S(core)	2.2719(13)	2.2618(5)	2.262(8)	2.287(3)
avg Fe–S(thiolate)	2.2431(14)	2.2239(6)	2.206(7)	2.287(3)
avg S(thiolate)–C	1.784(5)	1.7786(19)	1.90(3)	1.772(10)
	$[Fe_4S_4(SMes)_4]^{2-c}$		$[Fe_4S_4(SPh)_4]^{2-d}$	$[Fe_4S_4(SPh)_4]^{3-e}$
oxidation state		$[Fe_4S_4]^{2+}$		$[Fe_4S_4]^{1+}$
avg Fe–Fe	2.760(5)		2.736(3)	2.744(17)
avg Fe–S(core)	2.286(5)		2.286(5)	2.309(6)
avg Fe–S(thiolate)	2.274(6)		2.263(3)	2.294(10)
avg S(thiolate)–C	1.778(14)		1.771(2)	1.751(26)

[a]Reference 10. [b]Reference 23. [c]Reference 24. [d]Reference 25. [e]Reference 17.

distances, ranging from 2.7324(4) to 2.7985(10) Å and from 2.2618(5) to 2.2819(11) Å, respectively, are shorter than those of cluster **1** (Fe–Fe, 2.8044(4)–2.9203(7) Å; Fe–S, 2.2620(7)–2.3199(7) Å).[11,12] Whereas the mean Fe–S(core) and Fe–S(thiolate) distances are similar between [Na(THF)] **2a** and [N^{n}Bu$_4$]**2a**, the S6–Na interaction (2.894(3) Å) in [Na(THF)]**2a** leads to the longer Fe2–S6 distance (2.2615(9) Å) relative to the other Fe–S(thiolate) distances (2.2128(10)–2.2445(15) Å).

The averaged Fe–Fe, Fe–S, and S–C distances of clusters **2a–e**, $[Fe_4S_4(STip)_4]^-$,[10] $[Fe_4S_4(SDpp)_4]^{2-}$,[23] $[Fe_4S_4(SMes)_4]^{2-}$ (Mes = mesityl),[24] $[Fe_4S_4(SPh)_4]^{2-}$,[25] and $[Fe_4S_4(SPh)_4]^{3-}$[17] are listed in Table 2. A comparison of the mean Fe–Fe distances between $[Fe_4S_4(SDpp)_4]^-$ (**2e**, 2.7324(4) Å) and $[Fe_4S_4(SDpp)_4]^{2-}$ (2.759(2) Å) indicates that the higher oxidation state leads to slightly shorter Fe–Fe distances. A similar comparison can be made with the known $[Fe_4S_4]^{2+/+}$ clusters, $[Fe_4S_4(SPh)_4]^{2-}$ (2.736(3) Å) and $[Fe_4S_4(SPh)_4]^{3-}$ (2.744(17) Å), although their difference is within the standard deviations. The variety of thiolate substituents affects the mean Fe–Fe distances more than the difference of the oxidation states, and the range of 2.7324(4)–2.7985(10) Å found for **2a–e** is larger than the differences caused by the change in oxidation states. A small influence of the oxidation states on Fe–Fe distances can be also seen in the volume of the Fe_4 tetrahedron. The values of clusters **2a–e** (2.40–2.58 Å^3) are slightly larger but not much different from the averaged values for $[Fe_4S_4(SAr)_4]^{2-}$ (Ar = aryl, 2.41 Å^3) and $[Fe_4S_4(SAr)_4]^{3-}$ (2.42 Å^3).[26] Much like the Fe–Fe distances, the Fe–S(core) distances become slightly shorter upon oxidation, that is, $[Fe_4S_4(SDpp)_4]^-$ (**2e**, 2.2618(5) Å) vs $[Fe_4S_4(SDpp)_4]^{2-}$ (2.287(3) Å) and $[Fe_4S_4(SPh)_4]^{2-}$ (2.286(5) Å) vs $[Fe_4S_4(SPh)_4]^{3-}$ (2.309(6) Å). The slight shortening of the Fe–Fe and Fe–S(core) distances is consistent with the reduction of the ionic radius of iron atoms upon oxidation and is also in agreement with the theoretical analysis of the qualitative energy level scheme of $[Fe_4S_4(SR)_4]^{-/2-/3-}$ clusters, which suggested that the redox events occur in the Fe–Fe nonbonding and the Fe–S(core) antibonding orbitals.[27] The difference in Fe–S(thiolate) distances between two oxidation states, **2e** (2.2239(6) Å) and $[Fe_4S_4(SDpp)_4]^{2-}$ (2.287(3) Å), is larger than those found in the Fe–Fe and Fe–S(core) distances and is also larger than the difference in Fe–S(thiolate) distances caused by changing the thiolate substituents in the same $[Fe_4S_4]^{3+}$ oxidation state, 2.206(7)–2.2439(13) Å for clusters **2a–e** and $[Fe_4S_4(STip)_4]^-$. Similarly, the difference in the Fe–N(SiMe$_3$)$_2$ distances among the three oxidation states of $[Fe_4S_4\{N(SiMe_3)_2\}_4]^{0/1-/2-}$ is larger than those found for the Fe–Fe and Fe–S(core) distances.[11,12] This indicates that the Fe–S(thiolate) and Fe–N(amide) distances are more flexible than the Fe–Fe and Fe–S(core) distances in the robust and structurally less flexible $[Fe_4S_4]$ core.

Cyclic Voltammograms of $[Fe_4S_4]^{3+}$ Clusters and the Influence of Bulky Substituents. An important function of HiPIP is the $[Fe_4S_4]^{3+}/[Fe_4S_4]^{2+}$ redox process. Thus, the cyclic voltammograms (CVs) of $[Fe_4S_4]^{3+}$ clusters **2a–e**, $[Fe_4S_4(STip)_4]^-$, and $[Fe_4S_4(SPh)_4]^{2-}$ were measured to evaluate the influence of thiolates on redox potentials. The results are summarized in Table 3, and Figure 4 shows the CV diagram of **2c**. The origin of the weak feature around −0.4 V in Figure 4 is probably a decomposed compound derived from the $[Fe_4S_4]^{4+}$ species, because this feature was not observed in the CV measurement between −0.2 and −1.4 V. All measurements were carried out in THF in the presence of [N^{n}Bu$_4$][PF$_6$] as the supporting electrolyte, and the potentials were referenced

Table 3. Redox Potentials (vs Ag/AgNO$_3$) of Clusters 2a–e, $[Fe_4S_4(STip)_4]^-$, and $[Fe_4S_4(SPh)_4]^{2-}$ in THF

redox couple	$[Fe_4S_4]^{4+}/[Fe_4S_4]^{3+}$	$[Fe_4S_4]^{3+}/[Fe_4S_4]^{2+}$	$[Fe_4S_4]^{2+}/[Fe_4S_4]^{+}$
2a	0.08	−0.82	
2b		−0.86	
2c	0.08	−0.84	
2d		−0.74	
2e		−0.63	−1.77
$[Fe_4S_4(STip)_4]^-$		−0.53	−1.71
$[Fe_4S_4(SPh)_4]^{2-}$		−0.21	−1.30

dx.doi.org/10.1021/ic402890k | Inorg. Chem. 2014, 53, 4000–4009

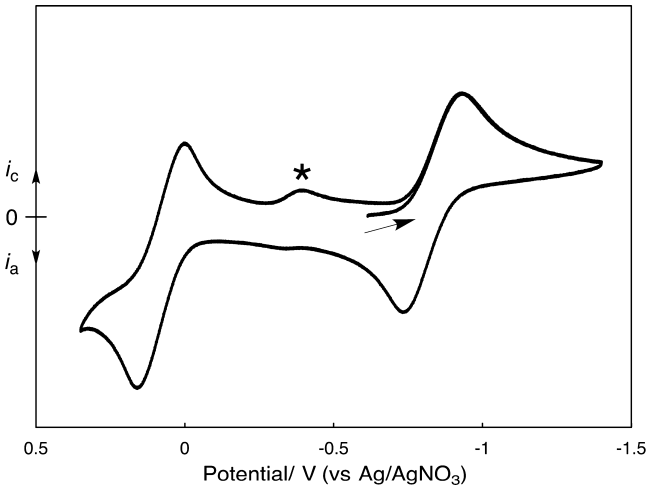

Figure 4. Cyclic voltammogram of $[N^nBu_4]$**2c**. Conditions: sample concentration, 3 mM in THF; supporting electrolyte, 0.3 M $[N^nBu_4][PF_6]$; working electrode, glassy carbon; counter electrode, Pt. The potential sweep was started at −0.614 V in the negative-going direction. The weak feature at −0.4 V (*) appears only after the scanning at $E_{1/2}$ = 0.08 V.

to $Ag/AgNO_3$. The Ag/Ag^+ reference was used instead of Fc/Fc^+ (Fc = $(C_5H_5)_2Fe$) because the $[Fe_4S_4]^{4+}/[Fe_4S_4]^{3+}$ process was obscured by the Fc/Fc^+ redox couple. Since a large excess of N^nBu_4 cation was present in the CV measurements, we speculate that the cation exchange from Na to N^nBu_4 occurs for [Na(THF)]**2a** and [Na(THF)]**2b**.

The $[Fe_4S_4]^{3+}/[Fe_4S_4]^{2+}$ redox couple in THF was observed at $E_{1/2}$ = −0.82 V (**2a**; R = Dmp), −0.86 V (**2b**; R = Tbt), −0.84 V (**2c**; R = Eind), −0.74 V (**2d**; R = Dxp), −0.63 V (**2e**; R = Dpp), and −0.53 V ($[Fe_4S_4(STip)_4]^-$). These $E_{1/2}$ values are significantly more negative than that with smaller benezenethiolates $[Fe_4S_4(SPh)_4]^{2-}$ ($E_{1/2}$ = −0.21 V). These comparisons suggest that the thiolate substituents have a major impact on the redox potentials. An interesting comparison can be made among clusters **2a** (R = Dmp), **2d** (R = Dxp), and **2e** (R = Dpp), since a wide range of redox potentials from −0.63 V (**2e**) to −0.82 V (**2a**) is achieved simply by changing the number of methyl groups incorporated in the 2,6-aryl moieties attached to the central phenyl ring. In contrast to this observation, the potentials for the oxidation of thiolate anions (E = −0.34 V for $^-$SDpp, −0.34 V for $^-$SDxp, and −0.36 V for $^-$SDmp) fall within a narrower range. Since these potentials indicate that the electronic effect of methyl groups on the 2,6-aryl moieties is indirect and small, we assume that the difference in potentials is more attributable to the steric effect of thiolate ligands.

Steric shielding of the $[Fe_4S_4]$ core by the bulky thiolates is a key to understanding the substituent dependence of the $[Fe_4S_4]^{3+}/[Fe_4S_4]^{2+}$ redox potentials. Figure 5 summarizes the redox potentials of clusters **2a**−**e**, $[Fe_4S_4(STip)_4]^-$, and $[Fe_4S_4(SPh)_4]^{2-}$ in descending order of the $[Fe_4S_4]^{3+}/[Fe_4S_4]^{2+}$ couple. With $[Fe_4S_4(SPh)_4]^{2-}$ as a standard, the series of clusters can be categorized into two groups. One group includes clusters having superbulky substituents, **2b** (R = Tbt), **2c** (R = Eind), and **2a** (R = Dmp). The other consists of clusters bearing moderately bulky substituents, **2d** (R = Dxp), **2e** (R = Dpp), and $[Fe_4S_4(STip)_4]^-$. As can be seen from the space-filling models of clusters **2a**−**e** (Figure 6), the bulky substituents nearly encapsulate the cluster anion, indicating that the latter group (R = Dxp, Dpp, Tip) has more space among substituents compared with the former group (R = Tbt, Eind, Dmp). We speculate that the degree of encapsulation is a major factor of the substituent-dependent redox properties found in the comparison of clusters **2a**−**e** and $[Fe_4S_4(STip)_4]^-$. Encapsulation of the $[Fe_4S_4]$ anion hinders its contact with

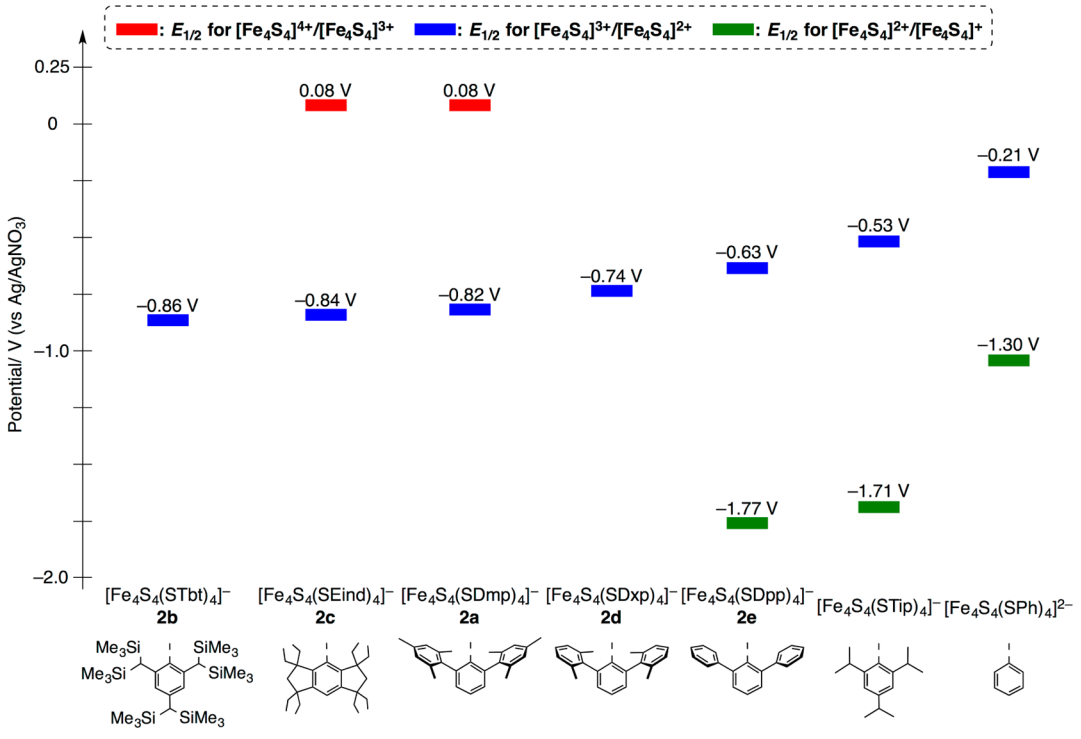

Figure 5. Redox potentials of clusters **2a**−**e**, $[Fe_4S_4(STip)_4]^-$, and $[Fe_4S_4(SPh)_4]^{2-}$ in THF.

dx.doi.org/10.1021/ic402890k | Inorg. Chem. 2014, 53, 4000−4009

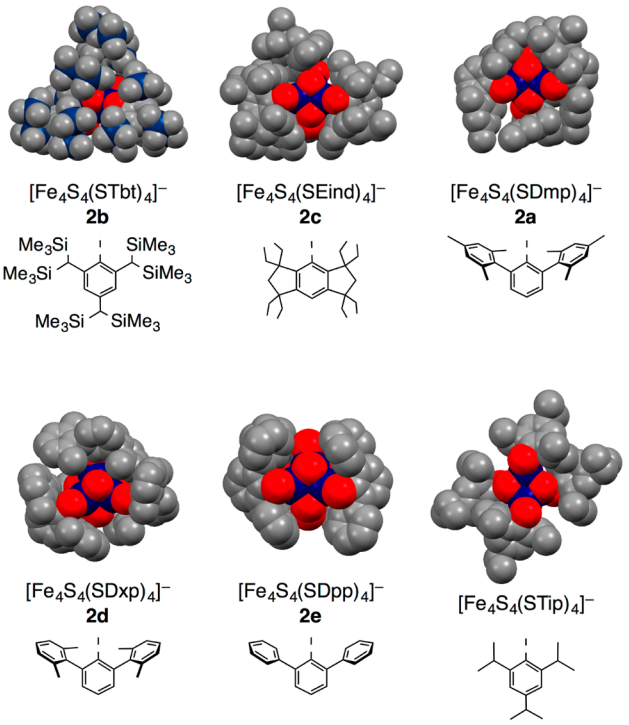

Figure 6. Space-filling descriptions of the crystal structures of clusters **2a**–**e** and $[Fe_4S_4(STip)_4]^-$.[10] Fe = blue, S = red, Si = light blue, carbon = dark gray.

solvent or the countercation and hence leads to a less efficient solvation and a decrease in charge neutralization by the interaction of the ion-pair. The electrochemical reduction of $[Fe_4S_4(SR)_4]^-$ gives the dianionic form $[Fe_4S_4(SR)_4]^{2-}$, which would require more efficient charge neutralization and solvation. Thus, for clusters **2a**–**e** and $[Fe_4S_4(STip)_4]^-$, steric shielding would destabilize the dianionic clusters $[Fe_4S_4(SR)_4]^{2-}$, and it also leads to the more negative potentials for the reduction of $[Fe_4S_4]^{3+}$ clusters $[Fe_4S_4(SR)_4]^-$. The negative shift of potentials by steric shielding is further supported by the potentials of the $[Fe_4S_4]^{2+}/[Fe_4S_4]^+$ redox couple observed for $[Fe_4S_4(SPh)_4]^{2-}$ ($E_{1/2}$ = −1.30 V), $[Fe_4S_4(STip)_4]^-$ ($E_{1/2}$ = −1.71 V), and **2e** (R = Dpp, $E_{1/2}$ = −1.77 V). Clusters **2a**–**d** only exhibit irreversible reduction waves from the $[Fe_4S_4]^{2+}$ state within the potential window of THF. Although it is difficult to quantify the coverage of the $[Fe_4S_4]$ core by substituents, these results suggest that the bulkiness of substituents controls not only the redox potentials but also the stable oxidation states of $[Fe_4S_4]$ clusters.

The steric effect of bulky thiolates in **2a**–**e** and $[Fe_4S_4(STip)_4]^-$ may be relevant to the hydrophobic environment around the $[Fe_4S_4]$ cluster of HiPIP. The $[Fe_4S_4]$ cluster in HiPIP is buried in a hydrophobic cavity consisting of alkyl and aromatic residues of amino acids, whereas the cluster in Fd is located around the protein surface and exposed to water. Therefore, the stable oxidation states of $[Fe_4S_4]$ clusters would be modulated by the adjustment of solvent accessibility to the clusters. This function of the hydrophobic cavity corresponds to the effect of steric shielding discussed above; that is, encapsulation of the $[Fe_4S_4]$ core stabilizes the $[Fe_4S_4]^{3+}$ oxidation state because bulky substituents would hinder the interaction between the cluster anion and the countercation or solvent molecules. Further, the substituent-dependent large shifts of the redox potentials observed in **2a**–**e** and $[Fe_4S_4(STip)_4]^-$ imply that a wide range of redox potentials for HiPIP is generated by even a small structural modulation of the hydrophobic cavity.

In contrast to the known $[Fe_4S_4]$ clusters, which usually exhibit the $[Fe_4S_4]^{2+}/[Fe_4S_4]^+$ redox couple, the reduced $[Fe_4S_4]^+$ state for clusters **2a**–**d** was not stable even in the CV time scale. Instead, the $[Fe_4S_4]^{4+}/[Fe_4S_4]^{3+}$ redox couple was observed for **2a** and **2c** at $E_{1/2}$ = +0.08 V, although the $[Fe_4S_4]^{4+}$ state has been unprecedented for synthetic and biological $[Fe_4S_4]$ clusters. This result is probably due to the large negative shift of redox potentials caused by the bulky thiolate ligands. The large negative shift would also result in the stabilization of the more oxidized $[Fe_4S_4]^{4+}$ state within the time scale of CV measurements, whereas synthesis of $[\mathbf{2a}]^+$ or $[\mathbf{2c}]^+$ via chemical oxidation has been unsuccessful thus far. The observation of the $[Fe_4S_4]^{4+}/[Fe_4S_4]^{3+}$ redox couple again shows the significant impact of the bulky thiolate ligands on the redox potentials.

CONCLUSIONS

A series of $[Fe_4S_4]^{3+}$ clusters, $[Fe_4S_4(SR)_4]^-$ (**2a**–**e**), modeling the oxidized form of HiPIP were synthesized from the ligand exchange reactions of $[Fe_4S_4\{N(SiMe_3)_2\}_4]^-$ (**1**) with 4 equiv of thiols (HSR), while bulky thiols were needed for stabilization of the products. This work offers a simple and convenient synthetic route to the $[Fe_4S_4]^{3+}$ clusters, and notably the precursor **1** is available from the one-pot reaction of $FeCl_3$, $NaN(SiMe_3)_2$, and NaSH, according to the synthetic procedure reported by Lee et al.[12] The structures of clusters **2a**–**e** were determined by X-ray crystallography, and they revealed that the Fe–S(thiolate) distances are more susceptible to redox than the Fe–Fe and Fe–S(core) distances of the $[Fe_4S_4]$ core. The CV measurements of clusters **2a**–**e** exhibited the $[Fe_4S_4]^{3+}/[Fe_4S_4]^{2+}$ redox couples, whose $E_{1/2}$ values were significantly more negative than that of $[Fe_4S_4(SPh)_4]^{2-}$. The large negative shift of the $[Fe_4S_4]^{3+}/[Fe_4S_4]^{2+}$ redox couples also enabled us to observe the uncommon $[Fe_4S_4]^{4+}/[Fe_4S_4]^{3+}$ redox couple for clusters **2a** and **2c**. We speculate that the steric effect of the bulky thiolate ligands is important for modulation of the redox potentials, because the bulky groups would efficiently hinder the electrostatic interaction between the cluster anion and the countercation, resulting in the destabilization of more negatively charged $[Fe_4S_4(SR)_4]^{2-}$ and $[Fe_4S_4(SR)_4]^{3-}$ clusters in the relatively reduced $[Fe_4S_4]^{2+}$ and $[Fe_4S_4]^+$ oxidation states.

EXPERIMENTAL SECTION

General Procedures. All reactions were manipulated using Schlenk techniques and a glovebox under a nitrogen atmosphere. Hexane, toluene, diethyl ether, dichloromethane, THF, CH_3CN, and hexamethyldisiloxane (HMDSO) were purified by the method of Grubbs,[28] where the solvents were passed over columns of activated alumina and a supported copper catalyst supplied by Hansen & Co., Ltd. The electrospray ionization mass spectra (ESI-MS) were recorded on a Bruker Micromass LCT TOF-MS or MicroTOF II at room temperature. UV–vis spectra were measured on a JASCO V560 spectrometer at room temperature. The EPR spectra of **2a**–**e** were recorded on a Bruker EMX-plus spectrometer at X-band frequencies. Cyclic voltammograms (CV) were recorded in THF at room temperature using glassy carbon as the working electrode with 0.3 M (for clusters **2a**–**e**, $[Fe_4S_4(STip)_4]^-$, and $[Fe_4S_4(SPh)_4]^{2-}$) or 0.2 M (for $^-$SDmp, $^-$SDxp, and $^-$SDpp) $[N^nBu_4][PF_6]$ as the supporting electrolyte. The potentials were measured against an $Ag/AgNO_3$ (0.01 M in CH_3CN) reference electrode separated from the working

dx.doi.org/10.1021/ic402890k | Inorg. Chem. 2014, 53, 4000–4009

compartment by a Vycor junction. ^{1}H and ^{13}C{H} NMR spectra were recorded on a JEOL ECA-600, and the data were analyzed by MestReNova software (version 8.1.2). ^{1}H NMR signals were referenced to the residual peaks of the solvents (CD_2Cl_2, δ 5.32; CD_3CN, δ 1.94). The ^{13}C chemical shifts were calculated by using the carbon signal for the deuterated solvent (CD_3CN, δ 118.20) as a reference. The ^{1}H NMR signal assignment was unsuccessful for $[Na(THF)][Fe_4S_4(SDmp)_4]$ ($[Na(THF)]$**2a**) and $[Na(THF)][Fe_4S_4(STbt)_4]$ ($[Na(THF)]$**2b**) because the number of signals was more than expected. This is probably due to the interaction between Na and the cluster anion. Elemental analyses were performed on a LECO-CHNS-932 elemental analyzer where the crystalline samples were sealed in tin capsules under nitrogen. $[N^nBu_4][PF_6]$ was purchased from TCI Co., Ltd., and used after recrystallization from THF. $[Na(THF)_2][Fe_4S_4\{N(SiMe_3)_2\}_4]$ ($[Na(THF)_2]$**1**),[11,12] HSDmp,[29] HSTbt,[30] HSEind,[31] HSDxp,[32] and HSDpp[33] were prepared according to the procedures described in the literature.

$[Na(THF)][Fe_4S_4(SDmp)_4]$, $[Na(THF)]$2a. A toluene (70 mL) solution of HSDmp (2.01 g, 5.80 mmol) was added to a toluene (10 mL) solution of $[Na(THF)_2][Fe_4S_4\{N(SiMe_3)_2\}_4]$ ($[Na(THF)_2]$**1**, 1.65 g, 1.42 mmol) at room temperature. The solution was stirred overnight before being evaporated to dryness. The black residue was extracted with a mixture of THF (1 mL) and toluene (30 mL), and the solution was centrifuged to remove a small amount of insoluble solid. The extract was concentrated to ca. 10 mL, and HMDSO (60 mL) was carefully layered. After slow diffusion at room temperature, black crystals of $[Na(THF)][Fe_4S_4(SDmp)_4]\cdot C_7H_8$ ($[Na(THF)]$**2a**$\cdot C_7H_8$, 1.89 g, 0.983 mmol, 69%) were obtained. UV−vis (THF): λ_{max} = 348 (ε 1.7 × 10^4), 446 nm (ε 1.4 × 10^4). Cyclic voltammetry (THF, room temperature): $E_{1/2}$ = 0.08 V ($[$**2a**$]^+/[$**2a**$]$), $E_{1/2}$ = −0.82 V ($[$**2a**$]/[$**2a**$]^-$). EPR (X-band, microwave 1.0 mW, 8 K): g = 2.076, 2.035, 2.018. ESI-TOF-MS (THF): m/z = 1732.4 (M^-). Anal. Calcd for $C_{100}Fe_4H_{108}NaOS_8\cdot C_7H_8$: C, 66.90; H, 6.09; S, 13.35. Found: C, 66.81; H, 6.33; S, 13.05.

$[N^nBu_4][Fe_4S_4(SDmp)_4]$, $[N^nBu_4]$2a. A toluene (12.5 mL) solution of HSDmp (358 mg, 1.03 mmol) was added to a toluene (6 mL) solution of $[Na(THF)_2][Fe_4S_4\{N(SiMe_3)_2\}_4]$ ($[Na(THF)_2]$**1**, 300 mg, 0.259 mmol) at room temperature. The solution was stirred overnight before being evaporated to dryness. The residue was extracted with THF (7.5 mL), and the black solution was mixed with a THF (12.5 mL) solution of $[N^nBu_4][PF_6]$ (100 mg, 0.258 mmol). The mixture was stirred overnight at room temperature. After evaporating to dryness under reduced pressure, the black residue was extracted with a mixture of toluene (15 mL) and dichloromethane (1.5 mL). The extract was centrifuged to remove an insoluble solid, and the solution was concentrated to *ca.* 3 mL. Black crystals of $[N^nBu_4][Fe_4S_4(SDmp)_4]\cdot(C_7H_8)_{1.5}$ ($[N^nBu_4]$**2a**$\cdot(C_7H_8)_{1.5}$, 373 mg, 0.176 mmol, 68%) grew at −30 °C. UV−vis (THF): λ_{max} = 343 nm (ε 2.1 × 10^4), 469 nm (ε 2.3 × 10^4). Cyclic voltammetry (THF, room temperature): $E_{1/2}$ = 0.09 V ($[$**2a**$]^+/[$**2a**$]$), $E_{1/2}$ = −0.83 V ($[$**2a**$]/[$**2a**$]^-$). EPR (X-band, microwave 1.0 mW, 8 K): g = 2.100, 2.051, 2.021. ESI-TOF-MS (THF): m/z = 1733.5 (M^-). ^{1}H NMR (CD_2Cl_2): δ 10.15 (8H, *m*-H), 6.75 (16H, *m*′-H), 4.21 (4H, *p*-H), 3.04 (8H, $NCH_2CH_2CH_2CH_3$), 2.55 (24H, *p*′−CH_3), 2.38 (48H, *o*′−CH_3), 1.66 (8H, $NCH_2CH_2CH_2CH_3$), 1.43 (8H, $NCH_2CH_2CH_2CH_3$), 1.03 (12H, $NCH_2CH_2CH_2CH_3$). Anal. Calcd for $C_{112}Fe_4H_{136}NS_8\cdot(C_7H_8)_{1.5}$: C, 69.58; H, 7.06; N, 0.66; S, 12.13. Found: C, 69.59; H, 7.00; N, 0.74; S, 11.87.

$[Na(THF)][Fe_4S_4(STbt)_4]$, $[Na(THF)]$2b. A pentane (20 mL) solution of HSTbt (605 mg, 1.03 mmol) was added to a pentane (10 mL) solution of $[Na(THF)_2][Fe_4S_4\{N(SiMe_3)_2\}_4]$ ($[Na(THF)_2]$ **1**, 300 mg, 0.258 mmol) at room temperature, and the solution was stirred overnight. After concentration to 10 mL, a small amount of black insoluble solid was filtered off. The solution was cooled at −30 °C to give $[Na(THF)][Fe_4S_4(STbt)_4]$ ($[Na(THF)]$**2b**, 190 mg, 0.0682 mmol, 26%) as black crystals. UV−vis (THF): λ_{max} = 459 nm (ε 2.0 × 10^4). Cyclic voltammetry (THF, room temperature): $E_{1/2}$ = −0.86 V ($[$**2b**$]/[$**2b**$]^-$). EPR (X-band, microwave 5.0 × 10^2 mW, 16 K): g = 2.100, 2.041. Anal. Calcd for $C_{112}Fe_4H_{244}NaOS_8Si_{24}$: C, 48.32; H, 8.83; S, 9.21. Found: C, 48.29; H, 8.52; S, 8.83.

$[N^nBu_4][Fe_4S_4(SEind)_4]$, $[N^nBu_4]$2c. The procedure for the synthesis of $[N^nBu_4]$**2c** is analogous to that of $[N^nBu_4]$**2a**, using $[Na(THF)_2]$**1** (500 mg, 0.431 mmmol), HSEind (715 mg, 1.72 mmol), and $[N^nBu_4][PF_6]$ (167 mg, 0.431 mmol). The residue derived from the reaction mixture was extracted with a mixture of pentane (15 mL) and toluene (15 mL) and was concentrated to ca. 5 mL. This solution was layered with hexane (20 mL) and was kept standing at room temperature. $[N^nBu_4][Fe_4S_4(SEind)_4]\cdot C_6H_{14}$ ($[N^nBu_4]$**2c**, 722 mg, 0.309 mmol, 72%) was obtained as black crystals. UV−vis (THF): λ_{max} = 342 nm (ε 1.4 × 10^4), 502 nm (ε 3.1 × 10^4). Cyclic voltammetry (THF, room temperature): $E_{1/2}$ = 0.08 V ($[$**2c**$]^+/[$**2c**$]$), $E_{1/2}$ = −0.84 V ($[$**2c**$]/[$**2c**$]^-$). EPR (X-band, microwave 1.0 × 10^{-1} mW, 16 K): g = 2.136, 2.043, 2.025. ESI-TOF-MS (THF): m/z = 2006.1 (M^-). ^{1}H NMR (CD_2Cl_2): δ 6.37 (4H, *p*-H), 5.55 (16H, CH_2CH_3), 3.84 (16H, CH_2CH_3), 3.07 (8H, $NCH_2CH_2CH_2CH_3$), 1.90 (16H, CCH_2C), 1.65 (16H, CH_2CH_3), 1.52 (16H, CH_2CH_3), 1.44 (48H, CH_2CH_3), 1.06 (12H, $NCH_2CH_2CH_2CH_3$), 0.77 (48H, CH_2CH_3). Anal. Calcd for $C_{128}Fe_4H_{216}NS_8\cdot C_6H_{14}$: C, 68.92; H, 9.93; N, 0.60; S, 10.99. Found: C, 68.51; H, 9.64; N, 0.56; S, 10.81.

$[N^nBu_4][Fe_4S_4(SDxp)_4]$, $[N^nBu_4]$2d. The reaction of $[Na(THF)_2]$ **1** (500 mg, 0.431 mmmol) with HSDxp (549 mg, 1.72 mmol) and $[N^nBu_4][PF_6]$ (167 mg, 0.431 mmol) gave a black solution, which was evaporated to dryness. The black residue was washed with hexane (15 mL) and was extracted with a mixture of toluene (25 mL) and dichloromethane (2 mL). After being concentrated to ca. 5 mL, the solution was stored at −30 °C. $[N^nBu_4][Fe_4S_4(SDxp)_4]$ ($[N^nBu_4]$**2d**, 368 mg, 0.197 mmol, 46%) was obtained as black crystals. UV−vis (THF): λ_{max} = 344 nm (ε 2.2 × 10^4), 466 nm (ε 2.6 × 10^4). Cyclic voltammetry (THF, room temperature): $E_{1/2}$ = −0.74 V ($[$**2d**$]/[$**2d**$]^-$). EPR (X-band, microwave 1.0 mW, 16 K): g = 2.109, 2.051. ESI-TOF-MS (THF): m/z = 1620.4 (M^-). ^{1}H NMR (CD_2Cl_2): δ 10.19 (8H, *m*-H), 7.02 (16H, *m*′-H), 6.58 (8H, *p*′-H), 4.01 (4H, *p*-H), 2.90 (8H, $NCH_2CH_2CH_2CH_3$), 2.45 (48H, *o*′-CH_3), 1.56 (8H, $NCH_2CH_2CH_2CH_3$), 1.45 (8H, $NCH_2CH_2CH_2CH_3$), 1.05 (12H, $NCH_2CH_2CH_2CH_3$). Anal. Calcd for $C_{104}Fe_4H_{120}NS_8$: C, 67.01; H, 6.49; N, 0.75; S, 13.76. Found: 66.64; H, 6.89; N 0.70; S, 13.34.

$[N^nBu_4][Fe_4S_4(SDpp)_4]$, $[N^nBu_4]$2e. The reaction of $[Na(THF)_2]$ **1** (500 mg, 0.431 mmmol) with HSDpp (452 mg, 1.72 mmol) and $[N^nBu_4][PF_6]$ (167 mg, 0.431 mmol) gave a black solution, which was evaporated to dryness. The black residue was washed with hexane (30 mL), and was extracted with a mixture of toluene (50 mL) and dichloromethane (5 mL). After being concentrated to ca. 15 mL, the solution was kept standing at room temperature to give black crystals of $[N^nBu_4][Fe_4S_4(SEind)_4]$ ($[N^nBu_4]$**2e**, 368 mg, 0.224 mmol, 52%). UV−vis (THF): λ_{max} = 465 nm (ε 2.1 × 10^4). Cyclic voltammetry (THF, room temperature): $E_{1/2}$ = −0.63 V ($[$**2e**$]/[$**2e**$]^-$), $E_{1/2}$ = −1.77 V ($[$**2e**$]^-/[$**2e**$]^{2-}$). EPR (X-band, microwave 1.0 mW, 16 K): g = 2.071, 2.028. ESI-TOF-MS (THF): m/z = 1396.4 (M^-). ^{1}H NMR (CD_2Cl_2): δ 10.03 (8H, *m*-H), 8.07 (16H, *m*′-H), 7.05 (8H, *p*′-H), 7.00 (16H, *o*′-H), 5.49 (4H, *p*-H), 2.88 (8H, $NCH_2CH_2CH_2CH_3$), 1.49 (8H, $NCH_2CH_2CH_2CH_3$), 1.29 (8H, $NCH_2CH_2CH_2CH_3$), 0.96 (12H, $NCH_2CH_2CH_2CH_3$). Anal. Calcd for $C_{88}Fe_4H_{88}NS_8$: C, 64.47; H, 5.41; N, 0.85; S, 15.65. Found: C, 64.31; H, 5.33; N, 0.86; S, 15.37.

$[Na][Fe_4S_4(STip)_4]$. Synthesis and spectroscopic data of $[N^nBu_4][Fe_4S_4(STip)_4]$ were reported by Millar et al.[10] The reaction of $[Na(THF)_2]$**1** (200 mg, 0.172 mmol) with HSTip (166 mg, 0.702 mmol) gave a black solution, which was evaporated to dryness. The black residue was washed with hexane (2 mL) and extracted with Et_2O (10 mL). After being evaporated to dryness, $[Na][Fe_4S_4(STip)_4]$ (30 mg, 13%) was obtained as a black solid. ESI-TOF-MS (THF): m/z = 1291.9 (M^-). Cyclic voltammetry (THF, room temperature): $E_{1/2}$ = −0.53 V ($[Fe_4S_4(STip)_4]^-/[Fe_4S_4(STip)_4]^{2-}$), −1.71 V ($[Fe_4S_4(STip)_4]^{2-}/[Fe_4S_4(STip)_4]^{3-}$).

$[N^nBu_4][Fe_4S_4(SPh)_4]$. This compound was prepared according to the procedure described in the literature.[34] ESI-TOF-MS (CH_3CN): m/z = 393.85 (M^{2-}). Cyclic voltammetry (THF, room temperature): $E_{1/2}$ = −0.21 V ($[Fe_4S_4(SPh)_4]^-/[Fe_4S_4(SPh)_4]^{2-}$), −1.30 V ($[Fe_4S_4(SPh)_4]^{2-}/[Fe_4S_4(SPh)_4]^{3-}$).

dx.doi.org/10.1021/ic402890k | *Inorg. Chem.* 2014, 53, 4000−4009

Table 4. Crystal Data for [Na(THF)][Fe_4S_4(SDmp)$_4$]·C_7H_8 ([Na(THF)]2a·C_7H_8), [N^nBu_4][Fe_4S_4(SDmp)$_4$]·(C_7H_8)$_2$ ([N^nBu_4]2a·(C_7H_8)$_2$), [Na(THF)][Fe_4S_4(STbt)$_4$] ([Na(THF)]2b), [N^nBu_4][Fe_4S_4(SEind)$_4$]·C_6H_{14} ([N^nBu_4]2c·C_6H_{14}), [N^nBu_4][Fe_4S_4(SDxp)$_4$]·(C_7H_8)$_3$ ([N^nBu_4]2d·(C_7H_8)$_3$), and [N^nBu_4][Fe_4S_4(SDpp)$_4$] ([N^nBu_4]2e)

	[Na(THF)]**2a**·C_7H_8	[N^nBu_4]**2a**·(C_7H_8)$_2$	[Na(THF)]**2b**
formula	$C_{107}H_{116}Fe_4NaOS_8$	$C_{123}H_{136}Fe_4NS_8$	$C_{112}H_{244}Fe_4S_8Si_{24}NaO$
formula wt (g mol^{-1})	2192.22	2108.30	2784.07
cryst syst	triclinic	triclinic	tetragonal
space group	$P\bar{1}$ (No. 2)	$P\bar{1}$ (No. 2)	$I4_1/a$ (No. 88)
a (Å)	14.4755(19)	15.765(2)	32.2442(9)
b (Å)	15.3293(18)	16.021(2)	
c (Å)	25.520(4)	25.024(3)	17.7890(7)
α (deg)	82.580(7)	83.258(5)	
β (deg)	87.684(7)	83.814(5)	
γ (deg)	61.671(4)	64.542(4)	
V (Å^3)	4941.4(12)	5665.6(11)	18495.0(11)
Z	2	2	4
D_{calcd} (g/cm^3)	1.291	1.238	1.000
max 2θ (deg)	55.0	55.0	55.0
no. of Refls measured	20 690	46 230	92 270
no. of data used ($I > 2.00\sigma(I)$)	16 067	25 523	10 571
no. of params refined	1037	1209	339
$R1$[a]	0.0727	0.0553	0.0947
$wR2$[b]	0.2142	0.1743	0.2454
GOF[c]	1.069	1.034	1.097
	[N^nBu_4]**2c**·C_6H_{14}	[N^nBu_4]**2d**·(C_7H_8)$_3$	[N^nBu_4]**2e**
formula	$C_{134}H_{206}Fe_4NS_8$	$C_{125}H_{134}Fe_4NS_8$	$C_{88}H_{78}Fe_4NS_8$
formula wt (g mol^{-1})	2310.98	2130.31	1629.46
cryst syst	monoclinic	triclinic	triclinic
space group	$P2_1/c$ (No. 14)	$P\bar{1}$ (No. 2)	$P2_1/n$ (No. 14)
a (Å)	17.359(2)	14.982(2)	20.1852(12)
b (Å)	24.540(3)	16.228(2)	18.3077(11)
c (Å)	31.797(4)	23.468(3)	22.3279(13)
α (deg)		94.710(3)	
β (deg)	92.8329(13)	92.628(2)	94.5234(9)
γ (deg)		100.580(3)	
V (Å^3)	13529(3)	5579.0(13)	8225.5(8)
Z	4	2	4
D_{calcd} (g/cm^3)	1.135	1.268	1.316
max 2θ (deg)	55.0	55.0	55.0
no. of Refls measured	137 618	69 030	98 601
no. of data used ($I > 2.00\sigma(I)$)	30 990	25 391	18 804
no. of params refined	1312	1193	934
$R1$[a]	0.0606	0.0687	0.0373
$wR2$[b]	0.1920	0.2499	0.0976
GOF[c]	1.098	1.097	1.216

[a] $I > 2\sigma(I)$, $R1 = \sum||F_o| - |F_c||/\sum|F_o|$. [b] Refined with all data, $wR2 = [\{\sum w(F_o^2 - F_c^2)^2\}/\sum w(F_o^2)^2]^{1/2}$. [c] GOF = $[\{\sum w(F_o^2 - F_c^2)^2\}/(N_o - N_p)]^{1/2}$, where N_o and N_p denote the numbers of reflection data and parameters.

NaSDmp. To a THF (10 mL) solution of HSDmp (301 mg, 0.869 mmol) was added Na (63 mg, 2.74 mmol). The suspension was stirred overnight at room temperature before filtration. The colorless solution was evaporated to dryness. The residue was washed with hexane (8 mL) to give NaSDmp (197 mg, 0.535 mmol, 62% yield) as a white powder. ESI-TOF-MS (CH_3CN): m/z = 345.2 ($^-$SDmp). ^{1}H NMR (CD_3CN): δ 6.82 (br, 4H, m'-H), 6.63 (dd, J = 7.9, 6.6 Hz, 1H, p-H), 6.55 (dd, J = 7.3, 0.4 Hz, 2H, m-H), 2.27 (s, 6H, m'-CH_3), 2.00 (s, 12H, o'-CH_3). ^{13}C{H} NMR (CD_3CN): δ 156.2, 144.9, 144.3, 136.7, 128.1, 126.9, 117.8, 21.1, 20.7. Cyclic voltammetry (THF, room temperature): E = −0.36 V (irreversible oxidation).

NaSDxp. The procedure for the synthesis of NaSDxp is analogous to that of NaSDmp, using HSDxp (301 mg, 0.945 mmmol) and Na (74 mg, 3.22 mmol). NaSDxp (259 mg, 0.761 mmol, 81% yield) was obtained as a white powder. ESI-TOF-MS (CH_3CN): m/z = 317.2 ($^-$SDxp). ^{1}H NMR (CD_3CN): δ 6.98 (br, 6H, m'-H, p'-H), 6.66 (dd, J = 7.3, 6.6, 1H, p-H), 6.57 (dd, J = 7.3, 0.5, 2H, m-H), 2.05 (s, 12H, o'-CH_3). ^{13}C{H} NMR (CD_3CN): δ 156.6, 148.0, 144.6, 137.0, 127.2, 126.6, 125.7, 117.5, 20.8. Cyclic voltammetry (THF, room temperature): E = −0.34 V (irreversible oxidation).

NaSDpp. To a THF (10 mL) solution of HSDpp (202 mg, 0.770 mmol) was added NaH (46 mg, 1.92 mmol). The suspension was stirred 4 h at room temperature before filtration. The afforded light yellow solution was evaporated to dryness. The residue was washed with hexane (4 mL) to give NaSDpp (181 mg, 0.639 mmol, 83% yield) as a white powder. ESI-TOF-MS (CH_3CN): m/z = 261.1 ($^-$SDpp). ^{1}H NMR (CH_3CN): δ 7.58 (m, 4H, o'- or m'-H), 7.26 (m, 4H, o'- or m'-H), 7.14 (m, 2H, p'-H), 6.83 (d, J = 7.4 Hz, 2H, m-H), 6.63 (dd, J = 7.6, 7.1, 1H, p-H). ^{13}C{H} NMR (CD_3CN): δ 157.2, 148.3, 145.4, 131.1, 128.6, 127.5, 125.7, 117.4. Cyclic voltammetry (THF, room temperature): E = −0.34 V (irreversible oxidation).

dx.doi.org/10.1021/ic402890k | Inorg. Chem. 2014, 53, 4000−4009

Table 5. Selected Bond Distances (Å) of [Na(THF)][Fe_4S_4(SDmp)$_4$] ([Na(THF)]**2a**), [N^{n}Bu$_4$][Fe_4S_4(SDmp)$_4$] ([N^{n}Bu$_4$]**2a**), [Na(THF)][Fe_4S_4(STbt)$_4$] ([Na(THF)]**2b**), [N^{n}Bu$_4$][Fe_4S_4(SEind)$_4$] ([N^{n}Bu$_4$]**2c**), [N^{n}Bu$_4$][Fe_4S_4(SDxp)$_4$] ([N^{n}Bu$_4$]**2d**), and [N^{n}Bu$_4$][Fe_4S_4(SDpp)$_4$] ([N^{n}Bu$_4$]**2e**)

	[Na(THF)]**2a**	[N^{n}Bu$_4$]**2a**	[Na(THF)]**2b**	[N^{n}Bu$_4$]**2c**	[N^{n}Bu$_4$]**2d**	[N^{n}Bu$_4$]**2e**
Fe1−Fe2	2.7282(8)	2.7498(8)	2.7996(8)[a]	2.2868(8)	2.8650(7)	2.7243(4)
Fe1−Fe3	2.8127(10)	2.7963(7)	2.7572(8)[b]	2.7758(8)	2.7773(8)	2.6815(4)
Fe1−Fe4	2.7894(8)	2.7542(8)	2.7996(8)[c]	2.7575(8)	2.7463(9)	2.6965(4)
Fe2−Fe3	2.7561(6)	2.7885(9)		2.7577(7)	2.8151(8)	2.7280(4)
Fe2−Fe4	2.7306(6)	2.8417(7)		2.7606(8)	2.7516(8)	2.7412(4)
Fe3−Fe4	2.7889(7)	2.7777(8)		2.7536(7)	2.8360(8)	2.8286(4)
Fe1−S1	2.2810(12)	2.2835(9)	2.2830(11)	2.2876(10)	2.3198(10)	2.2719(5)
Fe1−S2	2.2885(11)	2.2506(13)	2.3007(12)[d]	2.2757(9)	2.2724(11)	2.2697(5)
Fe1−S3	2.2316(11)	2.2725(12)	2.2619(11)[e]	2.1949(10)	2.2343(12)	2.2240(5)
Fe2−S1	2.3020(12)	2.2105(13)		2.2867(11)	2.2922(12)	2.2714(5)
Fe2−S2	2.2625(13)	2.2792(9)		2.2923(9)	2.2761(10)	2.2825(6)
Fe2−S4	2.2716(13)	2.2911(11)		2.2032(10)	2.2523(13)	2.2459(5)
Fe3−S1	2.2471(12)	2.2854(11)		2.2892(10)	2.2393(13)	2.2107(5)
Fe3−S3	2.3057(13)	2.2900(9)		2.2849(10)	2.2831(10)	2.2822(6)
Fe3−S4	2.2791(13)	2.2628(14)		2.2700(11)	2.3018(13)	2.2947(5)
Fe4−S2	2.2177(11)	2.2871(10)		2.2536(9)	2.2352(12)	2.2146(5)
Fe4−S3	2.2716(12)	2.2247(13)		2.2863(11)	2.2896(12)	2.2814(5)
Fe4−S4	2.2674(14)	2.2918(9)		2.2691(11)	2.2665(12)	2.2913(6)
Fe1−S5	2.2445(15)	2.2495(11)	2.2424(12)[f]	2.2343(11)	2.2401(14)	2.2162(5)
Fe2−S6	2.2615(9)	2.2392(12)		2.2280(10)	2.2472(11)	2.2365(5)
Fe3−S7	2.2408(11)	2.2523(13)		2.2407(9)	2.2540(13)	2.2198(5)
Fe4−S8	2.2128(10)	2.2444(12)		2.2199(10)	2.2303(12)	2.2238(6)

[a]Fe1−Fe1^1. [b]Fe1−Fe1^2. [c]Fe1−Fe1^3. [d]Fe1−S1^1. [e]Fe1−S1^2. [f]Fe1−S2.

X-ray Crystal Structure Determination. Crystal data and refinement parameters for [Na(THF)]**2a**, [Na(THF)]**2b**, [N^{n}Bu$_4$]**2a**, [N^{n}Bu$_4$]**2c**, [N^{n}Bu$_4$]**2d**, and [N^{n}Bu$_4$]**2e** are summarized in Table 4, and the selected bond distances of these clusters are listed in Table 5. Single crystals were coated with oil (Immersion Oil, type B, code 1248; Cargille Laboratories, Inc.) and mounted on loops (CryoLoop). Diffraction data were collected at −100 °C under a cold nitrogen stream on a Rigaku AFC8 equipped with a Mercury CCD detector or on a Rigaku RA-Micro7 equipped with a Saturn70 CCD detector, using graphite-monochromated Mo Kα radiation (λ = 0.710690 Å). Six preliminary data frames were measured at 0.5° increments of ω, to assess the crystal quality and preliminary unit cell parameters. The intensity images were also measured at 0.5° intervals of ω. The frame data were integrated using the CrystalClear program package, and the data sets were corrected for absorption using the REQAB program. The calculations were performed with the CrystalStructure program package. All structures were solved by direct methods and refined by full−matrix least-squares. Anisotropic refinement was applied to all non-hydrogen atoms except for the disordered atoms, and all hydrogen atoms were put at the calculated positions. An alert-A appears in the CIF-check program for [Na(THF)]**2a** because of the low completeness of data collection. This alert is inevitable because of the small size of crystals. An alert-B appears in the CIF-check program for [Na(THF)]**2b** because of the low crystal density. This is also inevitable because this alert comes from nontight packing in the crystal state.

■ ASSOCIATED CONTENT

Supporting Information

An X-ray crystallographic information file (CIF) for the structures of [Na(THF)]**2a**, [Na(THF)]**2b**, [N^{n}Bu$_4$]**2a**, [N^{n}Bu$_4$]**2c**, [N^{n}Bu$_4$]**2d**, and [N^{n}Bu$_4$]**2e**. This material is available free of charge via the Internet at http://pubs.acs.org.

■ AUTHOR INFORMATION

Corresponding Author

*E-mail: i45100a@nucc.cc.nagoya-u.ac.jp.

Notes

The authors declare no competing financial interest.

■ ACKNOWLEDGMENTS

This research was financially supported by Grant-in-Aids for Scientific Research (Nos. 18GS0207, 23000007, 23685015) and Grant-in-Aids for Scientific Research on Innovative Areas "Stimuli-responsive Chemical Species for Creation of Functional Molecules" (Nos. 24109003, 24109013, 25109522) from the Ministry of Education, Culture, Sports, Science and Technology, Japan. Kazuki Tanifuji thanks the JSPS for a Young Scientist research fellowship. We thank Roger E. Cramer (the University of Hawaii) for his help in the X-ray crystallographic analysis.

■ REFERENCES

(1) (a) Stephens, P. J.; Jollie, D. R.; Warshel, A. *Chem. Rev.* **1996**, *96*, 2491−2514. (b) Beinert, H.; Holm, R. H.; Münck, E. *Science* **1997**, *277*, 653−659. (c) Imsande, J. *Plant Physiol. Biochem.* **1999**, *37*, 87−97. (d) Beinert, H. *J. Biol. Inorg. Chem.* **2000**, *5*, 2−15. (e) Bentrop, D.; Capozzi, F.; Luchinat, C. Iron-sulfur Proteins. In *Handbook on Metalloproteins*; Bertini, I., Sigel, A., Sigel, H., Eds.; Marcel Dekker, Inc.: New York, 2001; pp 357−447.

(2) (a) Adman, E.; Warenpaugh, K. D.; Jensen, L. H. *Proc. Natl. Acad. Sci. U.S.A.* **1975**, *72*, 4854−4858. (b) Dey, A.; Jenney, F. E., Jr.; Adam, M. W. W.; Babini, E.; Takahashi, Y.; Fukuyama, K.; Hodgson, K. O.; Hedman, B.; Solomon, E. I. *Science* **2007**, *318*, 1464−1468.

(3) (a) Rayment, I.; Wesenberg, G.; Cusanovich, M. A.; Holden, H. M. *J. Mol. Biol.* **1992**, *228*, 672−686. (b) Dauter, Z. D.; Wilson, K. S.; Sieker, L. C.; Meyer, J.; Moulis, J.-M. *Biochemistry* **1997**, *36*, 16065−16073. (c) Liu, L.; Nogi, T.; Kobayashi, M.; Nozawa, T.; Miki, K. *Acta Crystallogr.* **2002**, *D58*, 1085−1091. (d) Mansy, S. S.; Xiong, Y.;

Hemann, C.; Hille, R.; Sundaralingam, M.; Cowan, J. A. *Biochemistry* **2002**, *41*, 1195−1201. (e) González, A.; Brenini, S.; Ciurli, S. *Acta Crystallogr.* **2003**, *D59*, 1582−1588. (f) Stelter, M.; Melo, A. M. P.; Hreggvidsson, G. O.; Hjorleifsdottir, S.; Saraiva, L. M.; Teixeira, M.; Archer, M. *J. Biol. Inorg. Chem.* **2010**, *15*, 303−313.
(4) (a) Meyer, T. E.; Przyshecki, C. T.; Watkins, J. A.; Bhattacharyya, A.; Simondsen, R. P.; Cusanovich, M. A.; Tollin, G. *Proc. Natl. Acad. Sci. U.S.A.* **1983**, *80*, 6740−6744. (b) Heering, H. A.; Bulsink, Y. B. M.; Hagen, W. R.; Meyer, T. E. *Biochemistry* **1995**, *34*, 14675−14686.
(5) Rao, P. V.; Holm, R. H. *Chem. Rev.* **2004**, *104*, 527−559 and references cited therein..
(6) (a) Ohno, R.; Ueyama, N.; Nakamura, A. *Inorg. Chem.* **1990**, *30*, 4887−4891. (b) Ueyama, N.; Yamada, Y.; Okamura, T.-A.; Kimura, S.; Nakamura, A. *Inorg. Chem.* **1996**, *35*, 6473−6484.
(7) Zhou, C.; Raebiger, J. W.; Segal, B. M.; Holm, R. H. *Inorg. Chim. Acta* **2000**, *300*, 892−902.
(8) Blonk, H. L.; Kievit, O.; Roth, E. K.-H.; Jordanov, J.; van der Linden, J. G. M.; Steggerda, J. J. *Inorg. Chem.* **1991**, *30*, 3231−3234.
(9) Kambayashi, H.; Nagao, H.; Tanaka, K. *Inorg. Chim. Acta* **1993**, *209*, 143−149.
(10) O'Sullivan, T.; Millar, M. M. *J. Am. Chem. Soc.* **1985**, *107*, 4096−4097.
(11) Ohki, Y.; Tanifuji, K.; Yamada, N.; Imada, M.; Tajima, T.; Tatsumi, K. *Proc. Natl. Acad. Sci. U.S.A.* **2011**, *108*, 12635−12640.
(12) Sharp, C. R.; Duncan, J. S.; Lee, S. C. *Inorg. Chem.* **2010**, *49*, 6697−6705.
(13) Ohki, Y.; Sunada, Y.; Tatsumi, K. *Chem. Lett.* **2005**, *34*, 172−173.
(14) (a) Ohki, Y.; Sunada, Y.; Honda, M.; Katada, M.; Tatsumi, K. *J. Am. Chem. Soc.* **2003**, *125*, 4052−4053. (b) Ohki, Y.; Ikagawa, Y.; Tatsumi, K. *J. Am. Chem. Soc.* **2007**, *129*, 10457−10465. (c) Ohta, S.; Ohki, Y.; Ikagawa, Y.; Suizu, R.; Tatsumi, K. *J. Organomet. Chem.* **2007**, *692*, 4792−4799. (d) Ohki, Y.; Imada, M.; Murata, A.; Sunada, Y.; Ohta, S.; Honda, M.; Sasamori, T.; Tokitoh, N.; Katada, M.; Tatsumi, K. *J. Am. Chem. Soc.* **2009**, *131*, 13168−13178. (e) Ohta, S.; Yokozawa, S.; Ohki, Y.; Tatsumi, K. *Inorg. Chem.* **2012**, *51*, 2645−2651. (f) Ohta, S.; Ohki, Y.; Hashimoto, T.; Cramer, R. E.; Tatsumi, K. *Inorg. Chem.* **2012**, *51*, 11217−11219.
(15) Aizman, A.; Case, D. A. *J. Am. Chem. Soc.* **1982**, *104*, 3269−3279.
(16) Papaefthymiou, V.; Millar, M. M.; Münck, E. *Inorg. Chem.* **1986**, *25*, 3010−3014.
(17) Laskowski, E. J.; Frankel, R. B.; Gillum, W. O.; Papaefthymiou, G. C.; Renaud, J.; Ibers, J. A.; Holm, R. H. *J. Am. Chem. Soc.* **1978**, *100*, 5322−5337.
(18) Heering, H. A.; Bulsink, Y. B. M.; Hagen, W. R.; Meyer, T. E. *Eur. J. Biochem.* **1995**, *232*, 811−817.
(19) Beinert, H.; Thomson, A. J. *Arch. Biochem. Biophys.* **1983**, *222*, 333−361.
(20) Cavazza, C.; Guigirarelli, B.; Bertrand, P.; Bruschi, M. *FEMS Microbiol. Lett.* **1995**, *130*, 193−200.
(21) Bertini, I.; Campos, A. P.; Luchinat, C.; Teixeira, M. *J. Inorg. Biochem.* **1993**, *52*, 227−234.
(22) (a) Shalmov, A. E.; Agashkin, O. V.; Yanovskii, A. I.; Struchkov, Y. T.; Logunov, A. P.; Revenko, G. P.; Bosyakov, Y. G. *J. Struct. Chem.* **1990**, *31*, 512−515. (b) Desiraju, G. R.; Steiner, T. *The Weak Hydrogen Bond in Structural Chemistry and Biology*; Oxford University Press: New York, 2001; pp 226−231.
(23) Lawson Daku, L. M.; Pcaut, J.; Lenormand-Foucaut, A.; Vieux-Melchior, B.; Iveson, P.; Jordanov, J. *Inorg. Chem.* **2003**, *42*, 6824−6850.
(24) Ueyama, N.; Sugawara, T.; Fuji, M.; Nakamura, A.; Yasuoka, N. *Chem. Lett.* **1985**, *14*, 175−178.
(25) Que, L., Jr.; Bobrik, M. A.; Ibers, J. A.; Holm, R. H. *J. Am. Chem. Soc.* **1974**, *96*, 4168−4178.
(26) Tan, L. L.; Holm, R. H.; Lee, S. C. *Polyhedron* **2013**, *58*, 206−217.
(27) Harris, S. *Polyhedron* **1989**, *8*, 2843−2882.
(28) Pangborn, A. B.; Giardello, M. A.; Grubbs, R. H.; Rosen, R. K.; Timmers, F. J. *Organometallics* **1996**, *15*, 1518−1520.
(29) (a) Ellison, J. J.; Ruhlandt-Senge, K.; Power, P. P. *Angew. Chem., Int. Ed.* **1994**, *33*, 1178−1180. (b) Ohki, Y.; Ohta, S.; Tatsumi, K. *Inorg. Synth.* **2010**, *35*, 137−143.
(30) Takeda, N.; Shimizu, D.; Tokitoh, N. *Inorg. Chem.* **2005**, *44*, 8561−8568.
(31) (a) Matsuo, T.; Suzuki, K.; Fukawa, T.; Li, B.; Ito, M.; Shoji, Y.; Otani, T.; Li, L.; Kobayashi, M.; Hachiya, M.; Tahara, Y.; Hashizume, D.; Fukunaga, T.; Fukazawa, A.; Li, Y.; Tsuji, H.; Tamao, K. *Bull. Chem. Soc. Jpn.* **2011**, *84*, 1178−1191. (b) Nishigaki, J.; Tsunoyama, R.; Tsunoyama, H.; Ichikuni, N.; Yamazoe, S.; Negishi, Y.; Ito, M.; Matsuo, T.; Tamao, K.; Tsukuda, T. *J. Am. Chem. Soc.* **2012**, *134*, 14295−14297.
(32) Luening, U.; Baumgartner, H. *Synlett* **1993**, *8*, 571−572.
(33) Bishop, P. T.; Dilworth, J. R.; Nicholson, T.; Zubieta, J. *J. Chem. Soc., Dalton Trans.* **1991**, 385−392.
(34) Christou, G.; Garner, C. D. *J. Chem. Soc., Dalton Trans.* **1979**, 1093.